Astronomy & Astrophysics

Reanalysis of the FEROS observations of HIP 11952[⋆,⋆⋆]
(Research Note)

A. Müller[1], V. Roccatagliata[2], Th. Henning[3], D. Fedele[4], A. Pasquali[5], E. Caffau[6], M. V. Rodríguez-Ledesma[3,7], M. Mohler-Fischer[3], U. Seemann[7], and R. J. Klement[8,3]

[1] European Southern Observatory, Alonso de Cordova 3107, Vitacura, Santiago, Chile
e-mail: amueller@eso.org
[2] Universitäts-Sternwarte München, Ludwig-Maximilians-Universität, Scheinerstr. 1, 81679 München, Germany
[3] Max-Planck Institut für Astronomie, Königstuhl 17, 69117 Heidelberg, Germany
[4] Max-Planck Institut für Extraterrestrische Physik, Giessenbachstrasse 1, 85748 Garching, Germany
[5] Astronomisches Rechen-Institut, Zentrum für Astronomie, Mönchhofstrasse, 12–14, 69120 Heidelberg, Germany
[6] Zentrum für Astronomie der Universität Heidelberg (ZAH), Landessternwarte, Königstuhl 12, 69120 Heidelberg, Germany
[7] Institut für Astrophysik, Georg-August-Universität, Friedrich-Hund-Platz 1, 37077 Göttingen, Germany
[8] Department of Radiotherapy and Radiation Oncology, Leopoldina Hospital, Gustav-Adolf-Str. 8, 97422 Schweinfurt, Germany

ABSTRACT

Aims. We reanalyze FEROS observations of the star HIP 11952 to reassess the existence of the proposed planetary system.
Methods. The radial velocity of the spectra were measured by cross-correlating the observed spectrum with a synthetic template. We also analyzed a large dataset of FEROS and HARPS archival data of the calibrator HD 10700 spanning over more than five years. We compared the barycentric velocities computed by the FEROS and HARPS pipelines.
Results. The barycentric correction of the FEROS-DRS pipeline was found to be inaccurate and to introduce an artificial one-year period with a semi-amplitude of 62 m s^{-1}. Thus the reanalysis of the FEROS data does not support the existence of planets around HIP 11952.

Key words. techniques: spectroscopic – planetary systems – techniques: radial velocities – stars: individual: HIP 11952

1. Introduction

In Setiawan et al. (2012) we reported the discovery of two planets around HIP 11952, a metal-poor star with [Fe/H] = −1.9 dex. We reported a long-period radial velocity (RV) variation of 290 d and a short-period variation of 6.95 d based on FEROS observations with the ESO/MPG 2.2 m telescope in La Silla. The spectroscopic analysis of the stellar activity revealed a stellar rotation period of 4.8 d. The observed RV variations had been associated to two planets with minimum planetary masses of 0.78 M_{Jup} and 2.93 M_{Jup} for the inner and the outer planet, respectively. In contrast to this result, based on HARPS N (mounted at the Telescopio Nazionale *Galileo*, La Palma) and HARPS (mounted at the ESO 3.6-m telescope in La Silla, Chile) observations, Desidera et al. (2013) did not find any evidence for planets around HIP 11952. In this research note

we reanalyze the RV signal of the FEROS data to clarify this discrepancy. In a first step we used the star HD 10700 to compare FEROS and HARPS measurements since there are many observations available for this object taken with both instruments. Recently, Tuomi et al. (2013) found a signal of five significant periodicities in the RV of HD 10700 that might be caused by a system of five planets with minimum masses between 2.0 and 6.6 $M_\oplus$. Since those signals are associated to RV variations below 1 m s^{-1}, the object is still suited to compare the FEROS (Kaufer et al. 1999) and HARPS (Mayor et al. 2003) data, taking into account the long-term precision of the FEROS RV measurements of about >10 m s^{-1}. The comparison reveals that the barycentric correction of the FEROS pipeline data is less accurate than needed for long-period RV monitoring. We applied a much more accurate correction to the FEROS data of HIP 11952 and show that with this improved correction there is indeed no evidence for planets around this object.

The paper is organized as follows: Sects. 2 and 3 present the observations and RV measurements of HD 10700 and HIP 11952, respectively. The effect of the inaccurate barycentric correction on FEROS RV measurements is presented in Sect. 4. The conclusions can be found in Sect. 5.

2. Radial velocity measurements of HD 10700

We analyzed a large data set of FEROS (117) and HARPS (153) spectra of the star HD 10700. The considered FEROS observations span a period of 5.6 years, while the HARPS
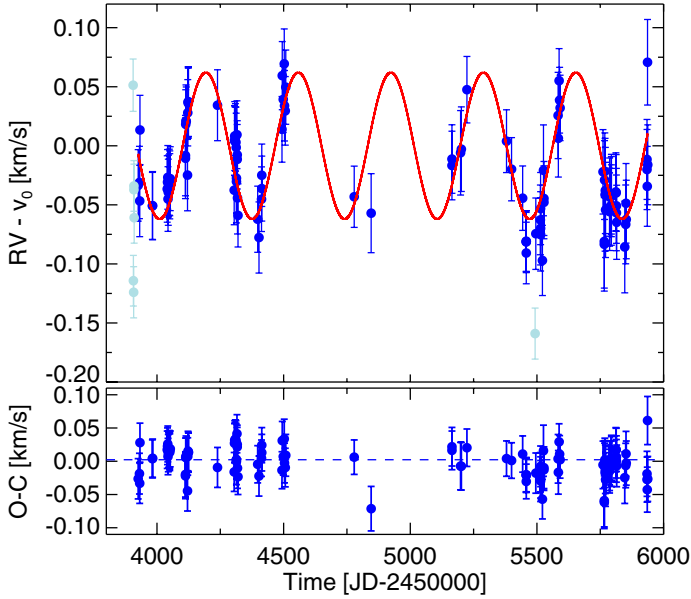
Fig. 1. RV measurements of HD 10700 using spectra reduced by FEROS-DRS. The red solid line is a sinusoidal fit with a period of 365.2 ± 0.2 days and a semi-amplitude of $62.0 \pm 1.1 \text{ m s}^{-1}$. Only spectra with a simultaneous ThAr exposure (blue data points) were considered for the fit. The present period of 365.2 days is caused by an inaccurate barycentric correction by the FEROS-DRS. The lower panel shows the residual of the fit.
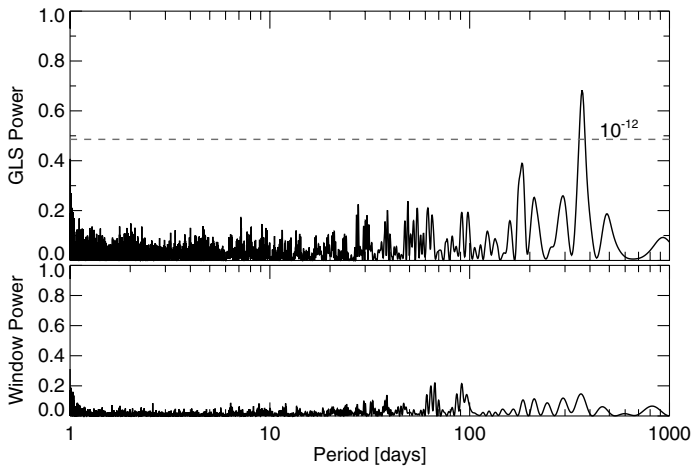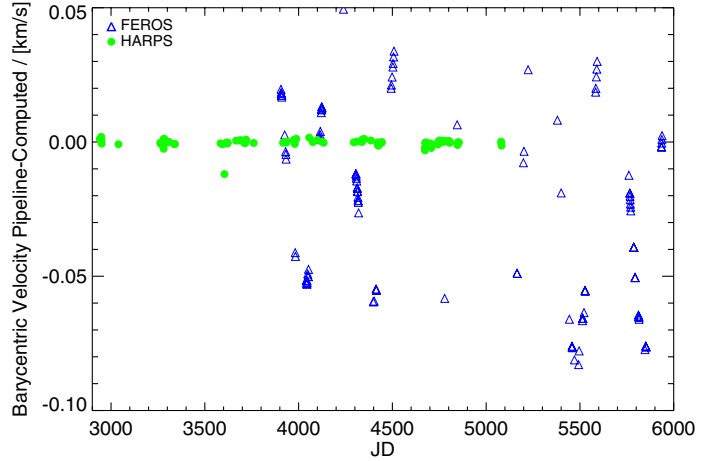

Fig. 2. Generalized Lomb-Scargle periodogram of the RV values of HD 10700. The horizontal dashed line indicates an FAP = 10^{-12}. A significant period of 365.2 days with an FAP of 7×10^{-24} is present in the FEROS data set.

observations cover 5.3 years. The measurement of the stellar RVs from FEROS and HARPS spectra was carried out using a self-written routine that cross-correlates the stellar spectra with a template spectrum. The template was a synthetic spectrum representing the stellar parameters of HD 10700. We computed the synthetic spectrum using SPECTRUM (Gray & Corbally 1994) with the ATLAS9 atmosphere models (Castelli & Kurucz 2004). Figure 1 shows the RV measurements based on FEROS data with the barycentric correction originally applied by the FEROS-DRS pipeline. Only exposures with a simultaneous ThAr spectrum were used to perform a sinusoidal fit. The radial velocity reveals a period of 365.2 days with a semi-amplitude of 62 m s^{-1}. Figure 2 shows the computed

Fig. 3. Difference of the computed and pipeline-provided barycentric correction for HD 10700. Green circles represent HARPS data and blue triangles represent FEROS data.

generalized Lomb-Scargle (GLS) periodogram (Zechmeister & Kürster 2009). The one-year period is clearly present and visible as the highest peak in the GLS. It has a false-alarm probability (FAP) of 7×10^{-24} computed by the GLS.

We found that the long period in the FEROS data arises because the barycentric correction of the FEROS-DRS pipeline was not accurate enough. In particular, it neglects the precession of the coordinates. We applied a more precise barycentric correction using the IDL code `baryvel.pro`[1]. The algorithm is based on Stumpff (1980) and is accurate to ~1 m s^{-1}.

In Fig. 3 we show the difference of the IDL-computed and pipeline-provided barycentric correction for HD 10700.

The comparison between the values computed by baryvel.pro and by the HARPS pipeline (in green) demonstrates that the adopted procedure computes the barycentric correction with the required accuracy, in contrast to the FEROS-DRS pipeline (in blue). The RMS-dispersion of the difference of the barycentric correction is 1.2 m s^{-1} and 34.6 m s^{-1} for HARPS-baryvel.pro and FEROS-baryvel.pro, respectively. Applying an accurate barycentric correction to the FEROS spectra, the RV values of HD 10700 are basically constant (see Fig. 4). No indication of either a one-year period or any other period is left. We also applied this routine to the HARPS data of HD 10700. The result is shown in Fig. 5. In addition to the higher signal-to-noise ratio (S/N) and spectral resolution of HARPS data with respect to the FEROS data, it should be considered that HARPS is an instrument fully optimized for high radial velocity precision (e.g. improved stability, vacuum tank).

3. Radial-velocity measurements of HIP 11952

3.1. Observations

The dataset of HIP 11952 includes the 77 observations presented in Setiawan et al. (2012) carried out from August 2009 until January 2011. We also included seven new FEROS observations not present in the analysis of Setiawan et al. (2012). All details about the observations are reported in Table B.1, including the S/N values measured at 5520 Å.

---

[1] Part of the IDL Astronomy Users Library available at http://idlastro.gsfc.nasa.gov
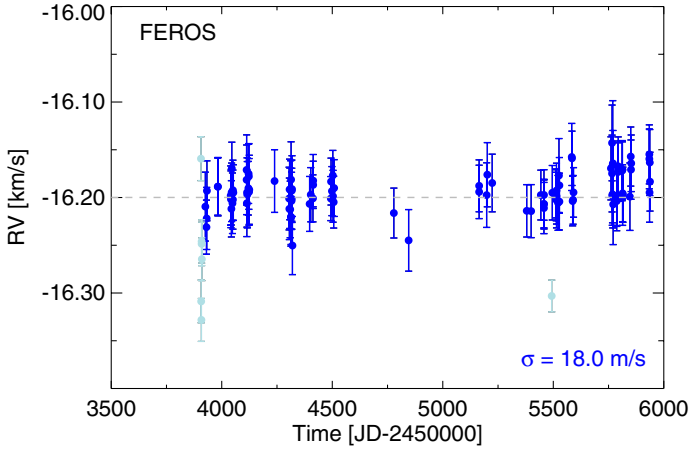
Fig. 4. RV measurements of HD 10700 using FEROS data. An accurate barycentric correction was applied. Light-blue data points indicate an observing mode where no simultaneous ThAr spectrum was taken.
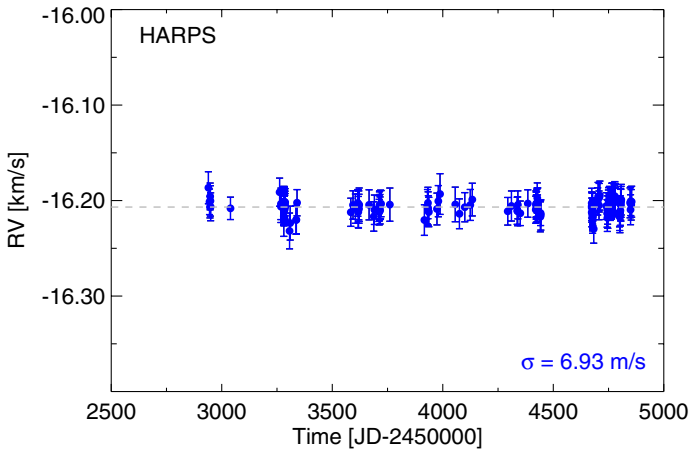

Fig. 5. RV measurements of HD 10700 using HARPS data.

We noticed that the data obtained between October 22 and 25, 2010 had poor ThAr+Ne frames.

3.2. Analysis

The RV of HIP 11952 was extracted by cross-correlating the stellar spectrum using two different templates and applying the newly computed barycentric correction. First, we used a synthetic spectrum created using the *Synthe* code based on ATLAS models with the stellar parameters determined in Setiawan et al. (2012) (e.g. $T_{\rm eff}$ = 5960 K, log g = 3.8 (g in cm s^{-2}), [Fe/H] = -1.95 dex). As a second approach, we used the stellar spectrum of HIP 11952 itself. We chose the observation with the highest S/N ($S/N = 170$) of all observations obtained on January 3, 2010. In both cases the RV was extracted in each FEROS order. The final RV was obtained using 15 echelle orders, ranging between 4143 Å and 6402 Å in wavelength. These orders have the highest S/N and are free of telluric lines. The RV values together with their errors are reported in Table B.1 for the synthetic template. We obtained similar results with the observed spectrum of HIP 11952. We obtained standard deviations of 36.1 m s^{-1} using the stellar template, and 39.3 m s^{-1} using the synthetic template (see Fig. 6).

We applied the GLS periodogram to the RV data to search for periodicities (see Fig. 7). We found no significant period in
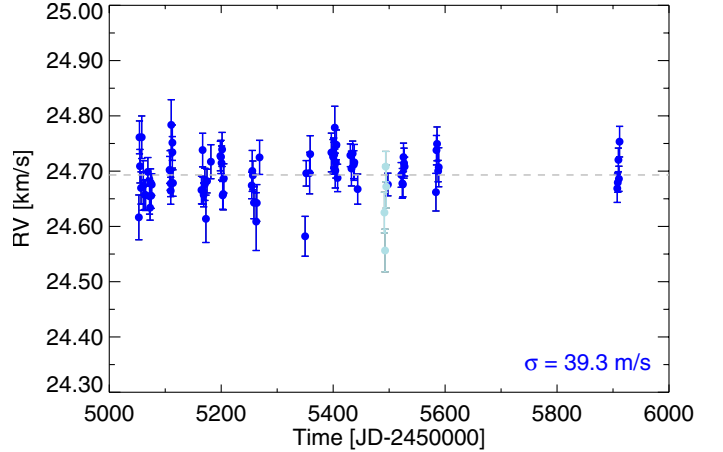
Fig. 6. RV measurements of the full data set of HIP 11952 containing 84 observations. The synthetic template was used. Light-blue data points indicate an observing mode where no simultaneous ThAr spectrum was taken. The standard deviation of the data set is 39 m s^{-1}, which resembles the size of the error bars.
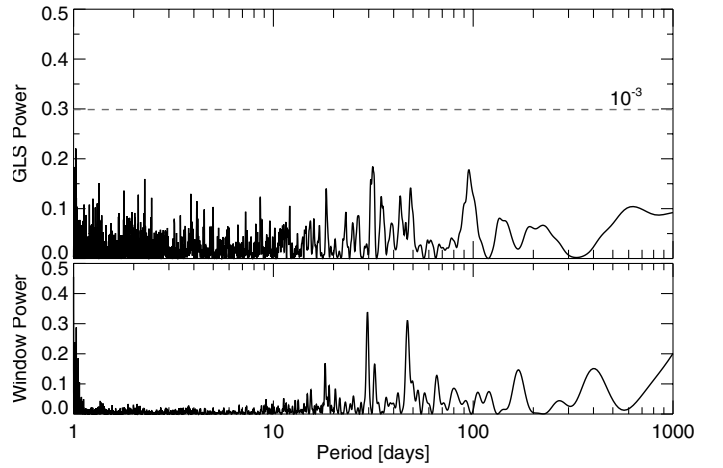
Fig. 7. GLS periodogram of the RV values of HIP 11952. There is no period present in the FEROS data set. The horizontal dashed line indicates an FAP = 10^{-3}.

the FEROS data. In particular, we found no sign of the 290 d and 6.95 d periods claimed in Setiawan et al. (2012), in agreement with the HARPS N result presented by Desidera et al. (2013).

4. Effect of the inaccurate barycentric correction on RV measurements

The inaccuracy of the barycentric correction of the pipeline might also affect previous RV studies carried out with FEROS. To investigate the effect on period searches using FEROS RV measurements without the applied accurate barycentric correction, we carried out a simulation using the following setup. As time basis we adopted the 77 epochs published in Setiawan et al. (2012), which cover 536 days. For periods between 5 and 350 days and velocity semi-amplitudes between 25 and 250 m s^{-1}, sine functions with noise were computed. Error bars with a mean value of ~17 m s^{-1} were added. The rms-dispersion of the difference for the noisy sine functions minus the sinus function without noise is ~17 m s^{-1}, too. The sinusoidal fit displayed in Fig. 1 was added to each computed sine function to account for the inaccurate barycentric correction by the

FEROS-DRS. For every setup we computed a GLS periodogram to determine whether the applied period could still be identified. Figure A.1 shows the computed GLS periodogram for each setup. The period and velocity semi-amplitude values used to compute the individual sine functions are displayed in the legend of the individual plots. The red dashed line represents the position of the period applied to compute the individual sine functions.

For pure sinusoidal RV variations, i.e. for variations without eccentricity, we draw the following conclusions:

– All periods can be identified for RV variations with semi-amplitudes greater than $\sim$150 m s^{-1}.
– For semi-amplitudes of around 100 m s^{-1} periods between $\sim$100 and $\sim$200 days cannot be clearly identified.
– If the semi-amplitude is smaller than 100 m s^{-1}, all periods present in the RV data set cannot be identified or are difficult to identify.
– Short periods $\lesssim$10 days can be detected reliably if the RV amplitude is greater than about twice the RV residuals.

5. Conclusions

In this research note we presented the analysis of the HARPS and FEROS spectra of the star HD 10700 and a new detailed re-analysis of the FEROS spectra of HIP 11952, in which we included seven new observations not presented in Setiawan et al. (2012). We found that

1. the barycentric correction of the FEROS pipeline was not accurate enough based on the analysis of HD 10700, and
2. the RV of HIP 11952 was recomputed applying a proper barycentric correction. As a result, no significant periodicity was found in HIP 11952.

This investigation clarifies the dsicrepancy between the FEROS-based RV measurements and the HARPS-based measurements and confirms the conlcusion that we see no evidence for planets around HIP 11952.

References

Castelli, F., & Kurucz, R. L. 2004, IAU Symp. 210, eds. N. Piskunov, et al., poster A20
Desidera, S., Sozzetti, A., Bonomo, A., et al. 2013, A&A, 554, A29
Gray, R. O., & Corbally, C. J. 1994, AJ, 107, 742
Kaufer, A., Stahl, O., Tubbesing, S., et al. 1999, The Messenger, 95, 8
Mayor, M., Pepe, F., Queloz, D., et al. 2003, The Messenger, 114, 20
Setiawan, J., Roccatagliata, V., Fedele, D., et al. 2012, A&A, 540, A141
Stumpff, P. 1980, A&AS, 41, 1
Tuomi, M., Jones, H. R. A., Jenkins, J. S., et al. 2013, A&A, 551, A79
Zechmeister, M., & Kürster, M. 2009, A&A, 496, 577

Appendix A: GLS periodograms for simulated RV measurements
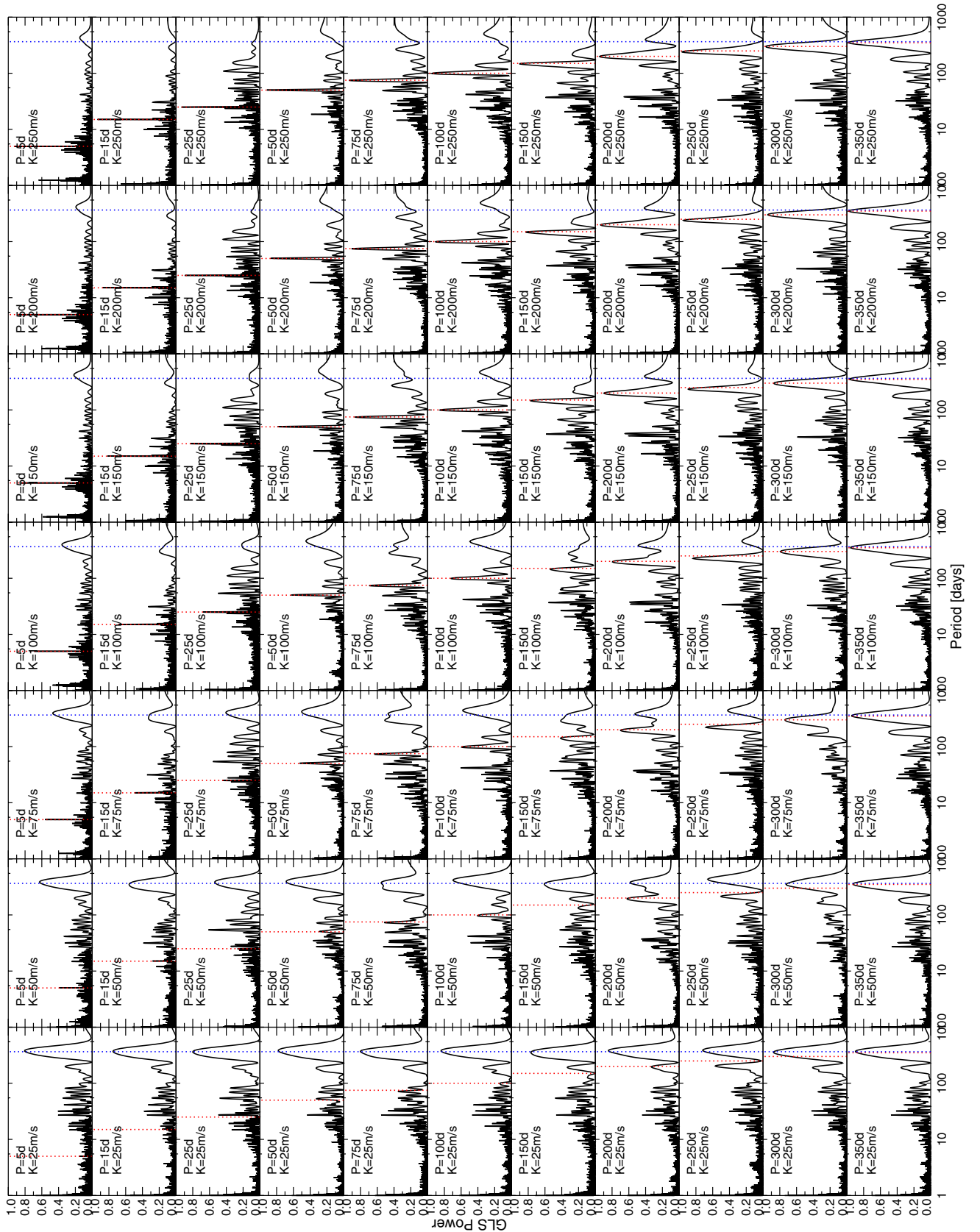
Fig. A.1. GLS periodogram for sine functions with different periods and velocity semi-amplitudes. The fit displayed in Fig. 1 was added to each sine function to account for the inaccurate barycentric correction by the FEROS-DRS. The period and velocity semi-amplitude used to compute the sine function are displayed in the legend of the individual plots. The red dashed line represents the position of the period applied to compute the sine function. The blue dashed line marks a one-year period.

Appendix B: Accompanying table

Table B.1. Observation log.

JD/[JD-240 000 d]	Exp. time/[s]	S/N	Airmass	Seeing/[arcsec]	RV/[m s^{-1}]	RVerr/[m s^{-1}]
55 052.83202	600	59	1.192	1.61	24 616.40	40.54
55 053.94928	600	62	1.069	0.83	24 761.19	29.71
55 054.90250	600	89	1.046	0.80	24 708.95	30.31
55 056.78339	900	70	1.385	1.24	24 669.57	29.18
55 057.94419	900	106	1.080	1.12	24 761.33	38.50
55 060.87386	960	41	1.052	2.16	24 674.07	44.89
55 063.83403	900	84	1.095	2.51	24 656.70	26.10
55 064.88164	900	146	1.045	0.94	24 656.71	27.92
55 068.89749	900	144	1.058	0.98	24 698.63	25.98
55 071.92782	900	154	1.128	0.79	24 654.55	32.41
55 072.90426	900	151	1.082	0.92	24 633.79	22.48
55 073.76953	900	152	1.207	1.01	24 679.67	24.56
55 074.91064	900	158	1.106	0.73	24 655.54	22.92
55 075.82762	900	127	1.057	1.30	24 675.65	19.60
55 107.78074	900	25	1.050	–	24 702.16	24.39
55 108.84721	800	57	1.192	1.02	24 701.29	35.77
55 109.76234	1200	118	1.046	1.07	24 664.45	24.41
55 109.78002	800	136	1.052	1.07	24 677.58	23.65
55 110.77245	800	53	1.050	0.75	24 783.65	45.61
55 112.76892	900	141	1.051	0.6	24 734.04	28.53
55 112.78081	800	141	1.061	0.5	24 751.45	32.03
55 113.76268	900	164	1.049	0.60	24 678.47	23.97
55 164.74363	900	150	1.495	0.63	24 665.81	25.04
55 166.74047	1000	151	1.522	0.54	24 738.16	30.37
55 167.63152	1000	169	1.063	0.66	24 664.44	24.32
55 168.64106	900	161	1.080	0.65	24 657.06	21.53
55 170.73747	1000	139	1.603	0.65	24 676.07	29.07
55 172.68382	900	115	1.244	0.84	24 613.74	42.86
55 174.66913	1200	170	1.211	1.21	24 681.98	21.38
55 181.54032	1000	157	1.054	0.70	24 717.05	30.76
55 198.52849	900	163	1.048	0.64	24 727.36	26.69
55 199.60741	900	171	1.231	0.71	24 725.67	30.05
55 200.62188	900	135	1.322	1.00	24 714.64	30.84
55 201.58493	900	150	1.164	1.28	24 739.26	30.82
55 202.61649	900	140	1.322	0.69	24 656.11	25.17
55 203.59183	900	132	1.211	1.21	24 658.71	28.74
55 204.63889	900	128	1.537	1.03	24 686.85	26.46
55 254.54266	900	67	2.132	1.06	24 674.11	24.01
55 255.52721	900	116	1.889	0.98	24 700.37	37.09
55 256.53307	900	133	2.045	0.82	24 692.35	26.00
55 258.52795	900	92	2.053	1.42	24 642.86	28.91
55 262.54577	329	73	2.757	0.62	24 608.74	52.33
55 263.54114*	546	103	2.294	0.80	24 642.47	33.24
55 268.50341	900	97	2.110	–	24 724.85	30.84
55 349.93534	800	60	1.889	–	24 582.13	36.08
55 351.92877	800	98	1.908	1.22	24 696.06	23.07
55 357.92508	800	95	1.718	–	24 696.46	37.54
55 358.92916	800	84	1.635	1.65	24 730.74	33.41
55 396.85224	1000	69	1.381	2.67	24 733.71	34.97
55 399.84778	800	125	1.363	1.12	24 725.86	31.32
55 400.91858	800	49	1.083	1.21	24 732.45	27.47
55 401.88071	800	80	1.172	1.24	24 729.91	22.26
55 402.87577	3000	46	1.147	3.45	24 778.73	38.66
55 403.80577	800	47	1.640	1.23	24 701.03	31.49
55 404.87298	800	143	1.171	0.49	24 715.76	28.34
55 405.85977	800	118	1.212	0.44	24 747.55	26.98
55 407.86952	800	101	1.155	1.08	24 687.73	24.75
55 430.81255	800	129	1.137	0.96	24 728.70	20.57
55 432.72912	800	71	1.611	1.40	24 704.66	31.44
55 434.83699	800	134	1.066	0.65	24 731.88	22.53

Notes. [*] FEROS observations of HIP 11952 not present in the analysis of Setiawan et al. (2012).

Table B.1. continued.

JD/[JD-240 000 d]	Exp. time/[s]	S/N	Airmass	Seeing/[arcsec]	RV/[m s^{-1}]	RVerr/[m s^{-1}]
55 436.85315	800	156	1.048	–	24 711.75	25.25
55 437.81918	600	128	1.082	0.40	24 715.80	32.50
55 443.74436*	800	62	1.265	0.96	24 667.47	27.30
55 491.59264	900	122	1.387	0.98	24 625.13	36.85
55 492.72899	900	110	1.051	0.94	24 556.40	38.67
55 493.79359	900	139	1.196	1.03	24 708.20	27.49
55 494.84164	900	130	1.511	1.15	24 672.08	38.83
55 497.80114	900	127	1.281	0.94	24 675.84	20.47
55 521.65675	900	139	1.057	1.07	24 693.18	22.35
55 523.64966	900	145	1.055	0.82	24 677.85	26.95
55 524.57918	900	152	1.083	0.90	24 675.97	22.39
55 525.65589	900	157	1.069	0.67	24 725.37	25.32
55 526.64926	900	165	1.063	0.54	24 714.46	27.10
55 527.63150	900	147	1.050	0.51	24 708.28	17.16
55 583.63214	900	126	1.944	0.64	24 661.91	34.04
55 584.59585	900	111	1.510	1.36	24 737.89	26.59
55 585.61612	1000	141	1.785	0.70	24 749.38	30.60
55 587.60350	1200	73	1.706	1.36	24 700.16	19.31
55 588.62755	900	82	2.122	–	24 707.08	35.28
55 907.60665*	900	159	1.064	0.61	24 668.73	25.30
55 908.51258*	900	142	1.115	0.85	24 679.38	17.49
55 909.64810*	900	139	1.170	0.94	24 720.42	21.30
55 910.51765*	900	129	1.092	–	24 686.16	22.72
55 911.64670*	900	147	1.184	1.19	24 753.35	27.62